This is a previous version of the article published in Optics & Laser Technology. 2021, 136: 106766. https://doi.org/10.1016/j.optlastec.2020.106766

Unveiling photophysical and photonic phenomena by means of optical gain measurements in waveguides and solutions

Luis Cerdán,[1] Marco Anni,[2] Maria Luisa De Giorgi,[2] Pedro G. Boj,[3] María Ángeles Díaz-García [4]*

[1]Instituto de Química y Física "Rocasolano", Consejo Superior de Investigaciones Científicas (CSIC), C/ Serrano 119, 28006, Madrid, Spain

[2]Dipartimento di Matematica e Fisica "Ennio de Giorgi", Universitá del Salento, via per Arnesano, 73100, Lecce, Italy

[3]Departamento de Óptica, Farmacología y Anatomía, Instituto Universitario de Materiales de Alicante y Unidad Asociada UA-CSIC, Universidad de Alicante, 03080, Alicante, Spain

[4]Departamento de Física Aplicada, Instituto Universitario de Materiales de Alicante y Unidad Asociada UA-CSIC, Universidad de Alicante, 03080, Alicante, Spain

Corresponding author e-mail: lcerdanphd@gmail.com

Abstract:

The increasing number of solution-processed laser compounds that can be implemented as low-cost, flexible, and/or integrated devices, makes necessary the development of reliable methods to delineate all their amplifying signatures and thus to open the door to appropriate cross-sample comparisons. Seeking to solve this problem, a new formalism to retrieve the losses and the optical gains from Amplified Spontaneous Emission (ASE) spectra as a function of the excitation density has been recently reported. In this manuscript, we explore the potential of this methodology to unveil relevant information on the photonic properties of the waveguiding devices and on the photophysics of the active materials. We demonstrate that the Variable Pump Intensity method opens the door to understand the relationship between the ASE thresholds and the optical gains and losses, it enables the extraction of the scattering/modal losses of the passive devices, and it can unveil the presence of leaky-modes and excited state absorption. In contrast, it does not perform too well in samples with multiple active species in its current implementation. We have substantiated all these findings using organic semiconductor thin films, several dye-doped polymer thin films and solutions of boron hydride.

Keywords: laser physics; gain materials; waveguides; amplified spontaneous emission

1. Introduction

The last decades have witnessed the advent of a myriad of new solution-processed laser compounds that can be implemented as low-cost, flexible, and/or integrated devices [1-3]. Much of this effort is and has been driven by the prospect of obtaining the long-sought after electrically pumped organic (or hybrid) laser, a device that it is finally becoming a reality [4, 5]. In the process of reaching this final goal, many advances have been done in optically pumped devices, either developing new organic, inorganic or hybrid active materials [1-3, 6-11], or optimizing the laser device fabrication and performance [1-3, 12-19].

Prior to checking their performance as thin film laser materials, each new compound is usually subjected to a series of experiments. In one of them the Amplified Spontaneous Emission (ASE) is measured under a variety of conditions with the idea to deeply characterize their optical gain and light amplification properties. By far the most popular and frequent experiment is the Variable Pump Intensity (VPI) method, which consists of collecting the photoluminescence spectra as a function of the pump intensity at a fixed stripe length. From this experiment one usually retrieves the pump value for which the ASE sets in, *i.e.*, the ASE threshold. This value is commonly used as a figure of merit for the goodness of a given compound as a laser material (the smaller, the better) [3].

An alternative figure of merit to benchmark the amplification performance of new laser materials is the optical gain, which is usually obtained from the well-known Variable Stripe Length (VSL) method and its variations [20, 21]. In this experiment, the ASE is measured as a function of the excitation stripe length at fixed pump intensity, and an adequate expression is fitted to those values to retrieve the optical gain. However, the most frequently used expression for this method is based on a series of approximations (mainly the assumption of homogeneity of gain across the excitation region and the lack of gain saturation), that most of the times are not fulfilled for active waveguides, thus casting doubts upon its reliability (see Ref. [22] and references therein). Aiming to develop a reliable method to correctly quantify the gain properties of active waveguides, one of us recently developed a new formalism based on the most frequent VPI method that allows retrieving the spectrally resolved

net optical gains at all pump values and, at the same time, the losses coefficient and an estimation of the ASE threshold [23]. The method is based on a newly found analytical expression for the growth of the ASE intensity, representing a generalization of that of the VSL method but that takes into account the most relevant spatio-temporal and photophysical effects that are overlooked by the VSL formalism.

Nevertheless, the full potential of this methodology, and its eventual limitations, to extract relevant information on the physics of the devices or the photophysics of the active materials have not been explored in depth. In order to fill this void, in this work we have confronted the VPI method with a series of situations that are usually encountered when analysing ASE in waveguides. In this sense, we have reanalysed datasets from previous experiments to reach a thorough understanding of the ASE properties of organic waveguides. In particular, we have first investigated the variation of the amplifying signatures with the active medium concentration and waveguide thickness using, respectively, polystyrene thin films doped with a Carbon-bridge oligo(*p*-phenylenevinylene) [24] and poly(9,9-dioctylfluorene) [25]. To check the performance of the VPI method in samples with more than one absorptive/emissive species, we have reanalysed a PMMA waveguide doped with the energy transfer pair Perylene Orange and Perylene Red [26], and a pHEMA waveguide doped with a rosamine in monomeric and aggregated form [27]. Finally, to exemplify the potentiality of the VPI method to detect the presence of Excited State Absorption (ESA) we have used ASE spectra obtained from a cyclohexene solution of the laser borane *anti*-$B_{18}H_{22}$ [28]. In the following sections, we will show that the VPI method helps in going beyond obtaining optical gains and calculating ASE thresholds that are in full agreement with the experimental ones. Actually, this method opens the door to understand the relationship between the ASE thresholds and optical gains and losses, it enables the extraction of the scattering losses of the passive devices, and it can unveil the presence of leaky-modes or excited state absorption. In contrast, since the current implementation of the VPI method assumes a single type of emitter, it does not perform too well in samples with multiple species (energy transfer pairs or aggregates).

2. Methods

Samples and ASE measurements: To test the performance and capabilities of the VPI method, we have analysed diverse samples based either on liquid solutions or thin films deposited on top of quartz substrates rendering slab waveguide amplifying devices. The ASE properties of the thin film samples were reported previously [24-27]. We have used, in particular: polystyrene thin films doped with a Carbon-bridge oligo(*p*-phenylenevinylene) [24]; thin films of the organic semiconductor polymer poly(9,9-dioctylfluorene) (PFO) [25]; PMMA waveguides doped with the energy transfer pair Perylene Orange and Perylene Red [26]; and pHEMA waveguides doped with a rosamine dye [27]. For a full description on the samples and ASE measurement set-up for the polymeric thin films, please refer to their corresponding original papers. Key aspects on the experimental details will be provided when needed.

The ASE spectra from solutions of the boron hydride *anti*-$B_{18}H_{22}$ [28] were freshly acquired for this manuscript using the experimental set-up schematically displayed and described in Fig. S1. In short, a 10 mM cyclohexene solution of *anti*-$B_{18}H_{22}$ was pumped at 355 nm with 7 ns pulses and with the spot conformed as a stripe of length 5 mm and width 200 microns. The edge emitted ASE was collected with a spectrograph coupled with a CCD detector.

VPI method: For the full details on the formalism, we refer the readers to ref. [23]. The analytical expression describing the growth of ASE intensity $I_{ASE}(\lambda,I_p,L)$ as a function of the wavelength, pump value (I_p; energy/density/intensity/flux/…) and stripe length (L) reads [23]:

$$I_{ASE}(\lambda, I_p, L) = \frac{\Omega(\lambda)\eta(I_p)}{\gamma(\lambda)\Delta n(I_p)-\alpha(\lambda)}\left(e^{(\gamma(\lambda)\Delta n(I_p)-\alpha(\lambda))L}-1\right) \quad (1a)$$

with

$$\Delta n(I_p) = \Delta n_0 \frac{\frac{I_p}{I^S_{p,1}}+\left(\frac{I_p}{I^S_{p,2}}\right)^m}{1+\frac{I_p}{I^S_{p,1}}+\left(\frac{I_p}{I^S_{p,2}}\right)^n} \quad (1b)$$

The function η and the effective population inversion Δn represent different measures of the temporally integrated spatially averaged excited state population. Note that η and Δn are normalized to unity at the maximum pump intensity of the experiment ($I_{p,max}$). In equation (1b), Δn_0 is a proportionality factor, $I^s_{p,1}$ and $I^s_{p,2}$ are a sort of saturation intensities, and m and n, with $m > n$, are exponents that determine how fast or slow the population inversion grows and saturates. The fluorescence parameter $\Omega(\lambda)$ contains information about the radiative properties of the active medium and is proportional to the fluorescence spectrum $F(\lambda)$. The total losses coefficient $\alpha(\lambda)$ accounts for the ground state absorption (GSA) and scattering/modal (SC) losses as:

$$\alpha = \alpha(\lambda) = \Gamma(\lambda)(\alpha_{SC}(\lambda) + \alpha_{GSA}(\lambda)) \tag{2}$$

where the mode confinement function $\Gamma(\lambda)$ accounts for all waveguiding effects as well as for the spatial overlap between the pump value variation across the film and the mode profile. The gross optical gain coefficient $\gamma(\lambda)$ is given by:

$$\gamma(\lambda) = \xi(\lambda)\Gamma(\lambda)(\alpha_{ST}(\lambda) + \alpha_{GSA}(\lambda) - \alpha_{ESA}(\lambda)) \tag{3}$$

where $\alpha_{ST}(\lambda)$, $\alpha_{GSA}(\lambda)$ and $\alpha_{ESA}(\lambda)$ are, respectively, the stimulated emission (ST), GSA and ESA coefficients. The spectral correction function $\xi(\lambda)$ accounts for the differences in amplification strength as a function of wavelength, and stems from the gain spatial homogeneity assumption and the differences in the temporal overlap between the population inversion and the photon flux at the different emission wavelengths [23].

An adequate fitting procedure allows obtaining $\alpha(\lambda)$, $\gamma(\lambda)$, $\eta(I_p)$ and the parameters associated to Δn (m, n, $I^s_{p,1}$ and $I^s_{p,2}$). The net optical gain g is subsequently obtained using the expression:

$$g = g(\lambda, I_p) = \gamma(\lambda)\Delta n(I_p) - \alpha(\lambda) \tag{4}$$

Finally, the ASE threshold (I_{th}) is calculated finding the pump value $I_p = I_{th}$ fulfilling the condition:

$$\frac{\left(e^{g(\lambda_{ASE}, I_{th})L} - 1\right)}{g(\lambda_{ASE}, I_{th})} = 2\frac{\left(1 - e^{-\alpha(\lambda_{ASE})L}\right)}{\alpha(\lambda_{ASE})} \tag{5}$$

All the ASE spectra datasets used along this manuscript were analysed using the VPI method as implemented in the GUI *AgL* [23]. The GUI can be obtained from the main author at no cost and can be freely distributed. The full details on the input parameters and the fitting results for the different samples analysed in this manuscript can be found in the Graphical Reports appended to the Supplementary Material.

3. Results and discussion

3.1 Concentration effects

When dealing with samples based on dyes or oligomeric compounds doped into passive matrices, one of the most typical procedures is to study the ASE properties as a function of the active medium concentration to find the optimal operation conditions (usually minimization of the ASE threshold) [29]. In this manuscript we will carry out this study in sets of ASE spectra obtained from polystyrene (PS) thin films doped with increasing amounts of COPV6, a Carbon-bridge oligo(*p*-phenylenevinylene) with six repeating units [24]. The complete fit results of all samples can be found in the "Graphical Reports" that have been appended to the Supplementary Material. In this section we will only highlight key aspect of this analysis.

We started by confirming whether the thresholds computed using the VPI method agreed with the visually obtained ones (pump intensity for which the Full Width Half Maximum, FWHM, collapses to half its maximum value). It is clear from Fig. 1a that the computed values reasonably reproduce the trends observed in the visually determined ones. Namely, the ASE threshold decreases when increasing the concentration, as there are more active centres contributing to the amplification process. Then, it increases again as a consequence of the quantum yield degradation induced by intermolecular aggregation [24]. It should be remarked that the VPI method allows retrieving a vast amount of information beyond the ASE threshold that was not described in the original paper.

The losses coefficient spectra display the expected nearly exponential decay (Fig. 1b) characteristic of the long wavelength tail of the absorption spectrum and a contribution of

modal/scattering losses evidenced by the presence of non-negligible losses above 570 nm (*i.e.*, in the molecule transparency window). Nevertheless, the losses at the ASE peak wavelength (around 582 nm) show a clear increase with the concentration (inset Fig. 1b), suggesting that at the ASE wavelength there is still a strong influence of the ground state absorption, probably due to the small Stokes shift in this material [24]. In principle one could expect a linear increase of the losses coefficient with the concentration [30] (whenever aggregation effects are negligible) and, on first consideration, this seems our case. Nevertheless, the waveguide mode confinement and its overlap with the gain distribution lead to a deviation from the linear dependency, which for these samples can be described as (see Appendix A):

$$\alpha(\lambda_{ASE}, C) \approx (\alpha_0 + \alpha_1 C) e^{-C/50} \tag{6}$$

with the concentration C in units of wt. %. With this expression we can re-assess how the losses change with the concentration. The inset of Fig. 1b shows the best fit of eq. (6) to the experimental values at the ASE wavelength. Note that, within the errors, the experimentally determined values follow the predicted sub-linear increase. The results of this fit can be used to unveil more information. For example, the fact that the losses coefficients at the ASE peak do not tend to zero as the concentration decreases suggests that in this region the presence of waveguiding effects and/or scattering is non-negligible (Figure 1b). In particular, the extrapolation of the fitted eq. (6) to C = 0 wt % enables estimating an inherent modal loss for the passive waveguides of approximately $\alpha(\lambda_{ASE},0) = \alpha_0 \approx 3.5$ cm^{-1}. In other words, in the ASE region, the losses due to reabsorption and the losses due to waveguiding or scattering effects are on par. In contrast, as we move towards the shorter wavelengths edge, the increase in the losses coefficient with the dye concentration is more pronounced (inset Fig. 1b). As it was otherwise expected, this means that in this region the losses are governed mostly by the ground state absorption.

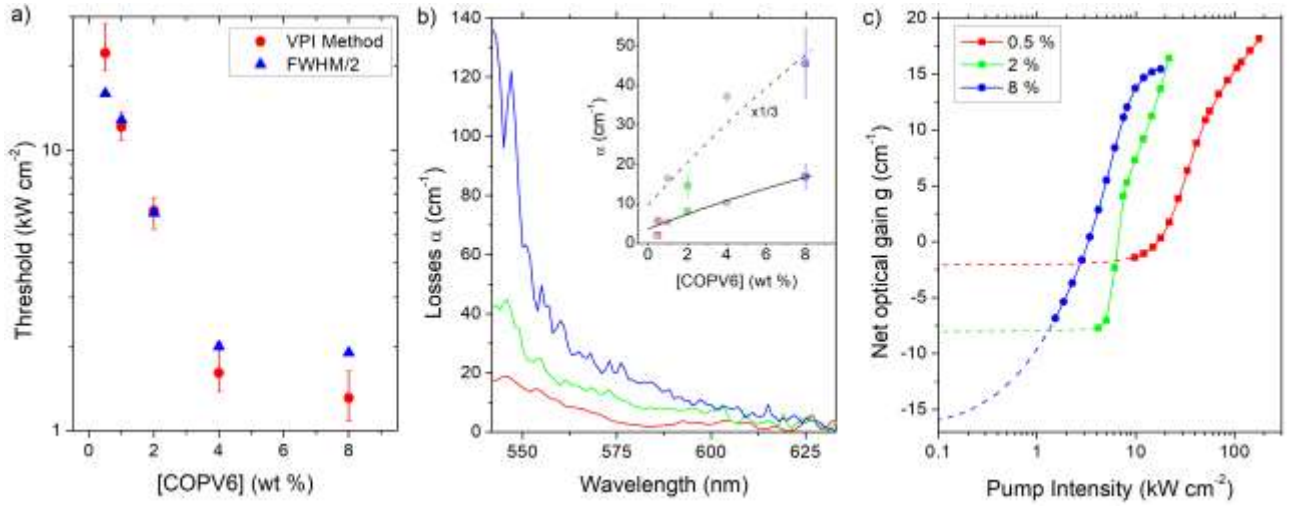

Figure 1: a) Computed (VPI method) and visually determined ASE thresholds as a function of COPV6 concentration. b) Losses coefficient spectra for COPV6/PS thin films for a selection of concentrations. Inset: Losses at the ASE peak (squares) and left-most (circles) wavelengths for increasing amounts of COPV6. The points are the experimental values and the lines are the best fits of eq. (6). The values for the left-most wavelength have been scaled for visualization purposes. c) Fitted net optical gain at ASE peak wavelength as a function of pump intensity for the same samples as in b). The dots and solid lines indicate, respectively, the range and positions of the experimental pump values, whereas the dashed lines represent the extrapolation towards zero pump intensity ($g = -\alpha$) using eq. (4). The colour codes in b) and c) match.

As it is seen in Figs. 1a and 1b, the samples 0.5 wt % and 8 wt % deviate from the general trend. On the one hand, their computed ASE thresholds show large discrepancies with the visually determined ones. In addition, the fitted losses coefficient at the peak wavelength for the sample with a 0.5 wt % seems to be underestimated, whereas that for the sample with an 8 wt % displays a very large error. These discrepancies could be ascribed to several combined factors: the noisy character of the ASE spectra used for the losses fit (see the corresponding Graphical Reports in the Supplementary Material); a low number of available ASE spectra (< 15 in some cases); the lack of enough ASE spectra below and close to threshold. This last factor can affect the fit results in two different ways. Firstly, if there is at least one ASE spectrum without any trace of amplification (or collapse in the FWHM), the shape of the losses spectra will be correctly retrieved. But the excess of ASE spectra above threshold with respect to the ones below (and close to) will have too much weight in the fit and will result in a distortion of the effective population inversion (Δn) dependency on the pump value and in a larger uncertainty for the losses. This modifies how the net optical gain changes

with the pump value and, in turn, affects the ASE threshold estimation (eq. (5)). Whereas all samples in this set suffer from this problem to a greater or lesser extent, that with an 8 wt % is the most seriously affected. This situation can be clearly appreciated in its fitted net optical gains as a function of the pump intensities (Fig. 1c). At the lowest pump intensity used for the experiment (full circles), the fit suggests that there is already a substantial level of amplification, *i.e*, $g >> -\alpha$. In contrast, the measured ASE spectrum at the lowest pump intensity shows that the amplification is insignificant, as there is almost no spectral collapse in the FWHM (see the corresponding Graphical Report in the Supplementary Material).

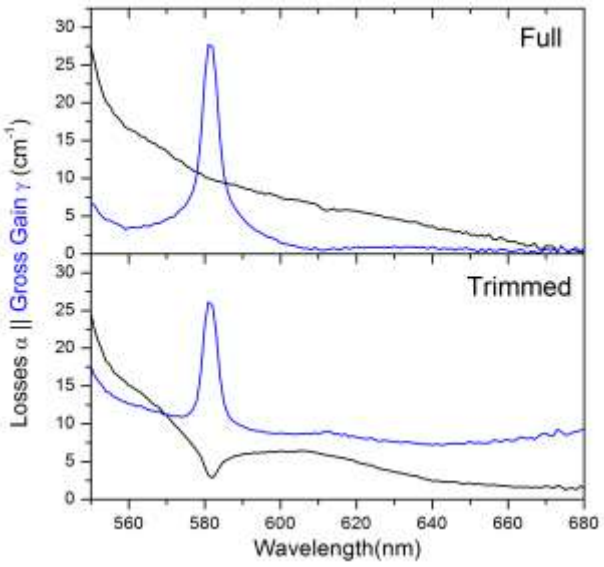

Figure 2: Fitted losses coefficient α and gross gain γ spectra using the full range of available ASE spectra ("Full") and removing those well-below threshold ("Trimmed").

The other way in which the lack of enough ASE spectra well-below threshold may affect the fit is that it may happen that the ASE spectrum at the lowest pump intensity displays already some level of amplification (or collapse in the FWHM). This situation may distort the fitted modal losses and, accordingly, the gross gain spectra. To visualize this effect, we first analysed a sample based on Perylene Orange [26] using all the experimentally available ASE spectra ("Full" dataset). Then, we removed those at the lowest pump intensities and repeated the analysis ("Trimmed" dataset). When using the full range of pump values, the losses coefficient spectrum follows the expected nearly

exponential decay (Fig. 2). In contrast, in the "Trimmed" case, the losses spectrum is highly distorted and displays a characteristic "dip" at the ASE peak wavelength, the losses value of which is very low. This distortion, in turn, results in a modification of the gross gain spectral shape (Fig. 2) and in an overestimation of the ASE threshold (see Graphical Reports in the SI). In the dataset corresponding to the compound COPV6, the only sample showing this distortion is that with a 0.5 wt% (Fig. 1a, although it is much better appreciated in the corresponding Graphical Report, see SI). This explains why its losses coefficient at the ASE peak is smaller than expected (Fig. 1b) and why its threshold is overestimated (Fig. 1a).

3.2 Thickness effects

Another parameter that it is usually explored when optimizing the ASE properties in waveguiding devices is the thickness of the thin film sustaining the emission. The analysis of this dependency becomes most useful to understand how the photonic environment or the mode confinement impinges in the device performance. In this manuscript we will carry out this study in sets of ASE spectra obtained from poly(9,9-dioctylfluorene) (PFO) thin films with thicknesses ranging from 48 to 660 nm (Samples S1 to S9) [25]. The complete fitting results and parameters of all samples can be found in the "Graphical Reports" that have been appended to the Supplementary Material. In this section we will limit ourselves to highlight key aspects of this analysis.

In the original paper, a comprehensive description of the ASE threshold as a function of the thickness was performed. As can be seen in Fig. 3a, the film with the lowest thickness displays a very high ASE threshold (with respect to this experimental set). Increasing the film thickness makes the threshold to sharply decrease, then to reach a minimum at around 150-200 nm, and finally to increase again steadily. A similar behaviour has been observed as well in diluted dye-doped inert polymer films [31]. It is worth digressing for a moment to explain this behaviour in more detail. For very low thicknesses, the waveguide mode is poorly confined, and the propagating field experiences high radiative losses and low amplification [25, 31]. Hence, they present very high thresholds. As the thickness is increased, the mode confinement improves, the losses are reduced and the population

inversion is used more efficiently, resulting in a sharp decrease in the ASE threshold to an optimum value. Nevertheless, as the thickness keeps increasing the evolution of the ASE threshold, and the physics behind this change, slightly differ for neat (highly absorbing) films and diluted (low-absorbing) films. In the latter, the threshold stops decreasing due to the activation of higher order modes that compete for the available gain and that contribute with higher radiative losses [31]. In neat films, to the activation of higher order modes, a reduction in the spatial overlap between the available gain and the mode(s) profile(s) due to the strong pump absorption is added [25]. Therefore, the ASE threshold not only stops decreasing but it starts increasing. Notice, though, that it is the combination of absorptive and refractive index properties of the waveguide structure what determines the differences in the ASE threshold trends, not the nature of the polymer film (neat or diluted).

Given the importance of this parameter, we first began performing the comparison of the ASE thresholds determined visually (start of FWHM collapse) and computationally (VPI method criterion eq. (5)). As it has been shown before (ref. [23] and Fig. 1a), the GUI *AgL* does a very good job finding the ASE threshold and the majority of the PFO samples did not impose any problem in this respect. The exception was that with a thickness of 48 nm (sample S1), as it lacked ASE spectra well below threshold, where there is no amplification. Accordingly, its losses coefficient spectrum displayed the characteristic dip at the ASE peak wavelength and its value at this wavelength was extremely low (see corresponding Graphical Report). As we have shown before, the threshold values, and the whole fit altogether, in this kind of datasets are not too reliable. As such, this sample will not be included in the following analyses.

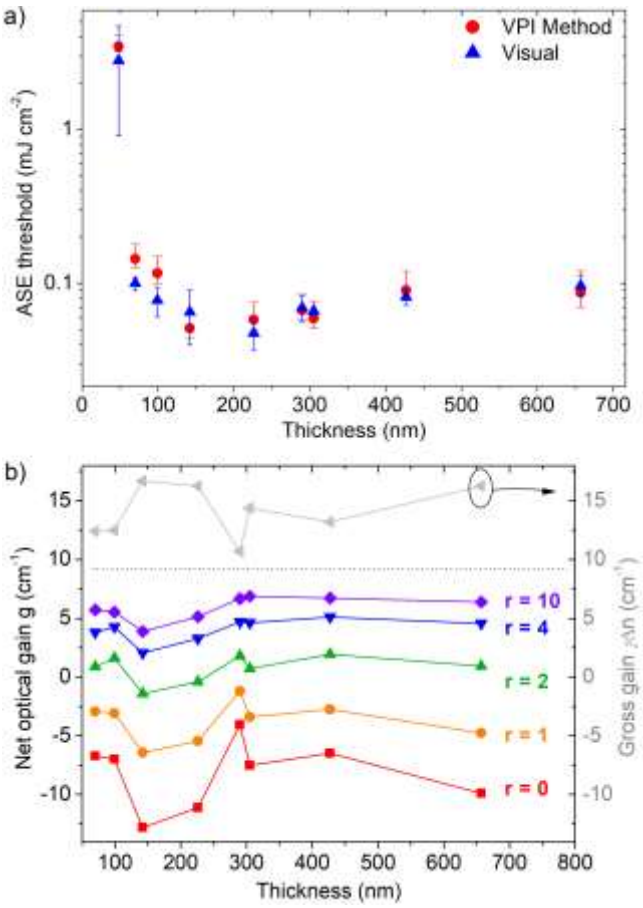

Figure 3: a) Computed (VPI method) and visually determined ASE thresholds in PFO films as a function of thickness. b) Effect of film thickness on the net optical gain *g* at different normalized pump values *r* assessed at the ASE peak wavelength. The curve for $r = 0$ corresponds to the opposite of the losses coefficient, *i.e.*, $g = -\alpha$. The upper-most trace represents the gross gain at $r = 10$ (scale in right axis).

Apart from the threshold, the VPI method allows retrieving a vast amount of information that was not described in the original paper. For example, it can provide a detailed description of the interplay between gain and losses and how they correlate with the threshold, and it can unveil the presence of spectrally resonant waveguiding effects (leaky-modes).

3.2.1 Correlation between gains, losses and thresholds

The fact that each sample has a threshold and that these thresholds are so different, makes the comparison of losses, gross gains and net gains highly challenging. The reason is that the losses are pump independent, but the gains are not. This is, at a given pump value, some samples might be well below threshold, others might be close to it, and others might be saturated. A way to compare the net

optical gain at different excitations, so that all samples are under similar amplification conditions, is to divide the pump values (I_{pump}) used for each sample by its threshold value (I_{th}), *i.e.*, $r = I_{pump}/I_{th}$. Nevertheless, to ensure proper comparisons with this normalized pump value, the pulse-width of the excitation beam should be larger than the photoluminescent lifetime to fulfil the quasi steady-state conditions and the stripe length should be long enough to make the threshold independent on the excitation area [32]. For this experiment, a pulse-width of 3 ns, much longer than the PFO lifetime [33], and a stripe length of 6.6 mm, which ensured that the threshold is invariant, were used [25]. Therefore, with the normalized pump value and under the previous conditions, we can safely compare the losses, the gross gain and the net gain as a function of the thickness at a similar excitation level.

Figure 3b represents the variation with the thickness of the net optical gains, at the ASE peak wavelength, for several values of the normalized pump value *r*. Notice that for $r = 0$, the net gain is minus the losses, *i.e.*, $g = -\alpha$. For comparison purposes, Figure 3b includes as well the value of the gross gain ($\gamma\Delta n$) at the maximum value of *r* used in this analysis. What is more remarkable in this plot is that even when the losses display large fluctuations (that will be clarified later on), the net optical gain becomes more and more independent on the thickness as the normalized pump value is increased. This independency contrasts with the huge modulation observed in the ASE threshold when changing the thickness. In fact, the representation of the ASE threshold vs. any of the parameters in Fig. 3b simply renders plots with scattered points (not shown), *i.e.*, there seems to be no correlation between threshold and gain or losses when changing the thickness.

Researchers in the field of laser materials are focused on trying to reduce the ASE threshold because we relate this reduction with an increase in the net optical gain, but this claim, as we have shown, does not seem to hold scrutiny, at least to what modifying the film thickness is concerned. This apparent contradiction is sustained independently by the analyses performed in the original paper [25] and in a previous publication [31]. It was shown that, for highly absorbing neat polymer films, the dependency of the ASE threshold on the film thickness can be described with a function

that is inversely proportional to the product of the mode confinement and the pump-to-mode overlap factor (eq. A1). For low absorbing dye-doped polymer films, as we have said before, this last term is not so relevant in general and one must invoke the excitation of higher-order guided modes to explain the observed variation [31]. Interestingly, for both types of films these parameters depend on the geometrical and optical properties of the waveguide structure and the absorptive properties of the active medium at the pump wavelength, but not on the photophysical properties in the emission range. It is probably in the proportionality factors where the gain and losses properties influence the threshold. Thus, this analysis suggests that there shouldn't be a strong correlation between the ASE threshold and the optical gain when modifying the thickness, as indeed happens.

As a final note on the interplay between losses, gain, and threshold, a cross-correlation analysis between the fitted parameters shows that the only variables that correlate are the losses α and the gross gains $\gamma\Delta n$ (cf. Fig. 3b). This positive correlation is also evidence from the comparison between the gross gain $\gamma\Delta n$ values at r = 10 and the losses values (net gain values at r = 0), and it is mainly due to the thickness independent values of the net optical gain at high excitation density and the strong thickness dependence of the losses, that we will cover in the next section.

3.2.2 Leaky-modes

The spectrally resolved analysis of the results obtained with the VPI method opens the door, in addition, to obtain relevant information on the photonic properties of the system. Attending to eq. (A2) and to the definition of the pump to mode overlap factor Γ_{PMO} (eq. (A1) and ref. [25]), the fitted losses coefficient should decrease exponentially with the thickness (provided that the scattering losses are constant). In contrast, the fitted values display a heavily fluctuating behaviour (Figure 3b). The inspection of the fitted losses spectra helps rationalizing this anomaly. In most cases, the losses spectrum should have a shape closely resembling an exponential decay, as the emission acquisition window usually overlaps the long wavelength tail of the absorption band. Clearly this is not the case for the set of PFO samples studied in this manuscript, as their absorption bands present a sort of resonances on top of the expected exponential decay (Fig. 4a and S2). These resonances are dragged

through the fitting procedure and are incorporated into the gross gain spectra as well. This spectral structure is not present in the absorption spectra measured in a spectrophotometer, which show the typical spectral shape for PFO [33]. This means that they are not actual absorbance features intrinsic to the material. Neither are they resulting from a lack of spectra well-below threshold (cf. Fig. 2), as the "dips" are not coincidental with the ASE peak (see graphical reports in SI). As explained before, an exception to this could probably be sample S1 (t = 48 nm). Anyway, having ruled out some kind of artefact in the software or fitting procedure, the only plausible explanation is the presence of waveguiding effects giving place to a modulation in the resulting ASE spectra.

This is much better observed inspecting the ASE spectra at the lowest pump energies (well-below threshold), where there is no amplification (Fig. 4b and S3). These spectra should resemble the fluorescence one but shifted to the red due to reabsorption effects. But this is not the case (notice how the bands positions and magnitudes change with the thickness). This effect can be explained by considering the coexistence of guided and leaky modes in the thin film structure [34, 35]. In the ray picture, leaky modes are those excited by the light emitted at an angle slightly below the critical angle for total internal reflection at the film/substrate interface. Under these circumstances, most of the light is reflected back to the film, and the rest leaks into the substrate, hence the name. The light confined within the film by Fresnel reflection keeps bouncing off both the film/air and film/substrate interfaces. At each reflection in the latter some light is leaked into the substrate. The total amount of emission leaked into the substrate will be determined by the constructive or destructive Fabry-Perot like interference of the multiple leaked beams. Thus, the in-substrate emission will depend on parameters such as the emission polarization, the film thickness, the emitted wavelength, the cladding, film and substrate refractive indices, the film absorption, and the detection angle.

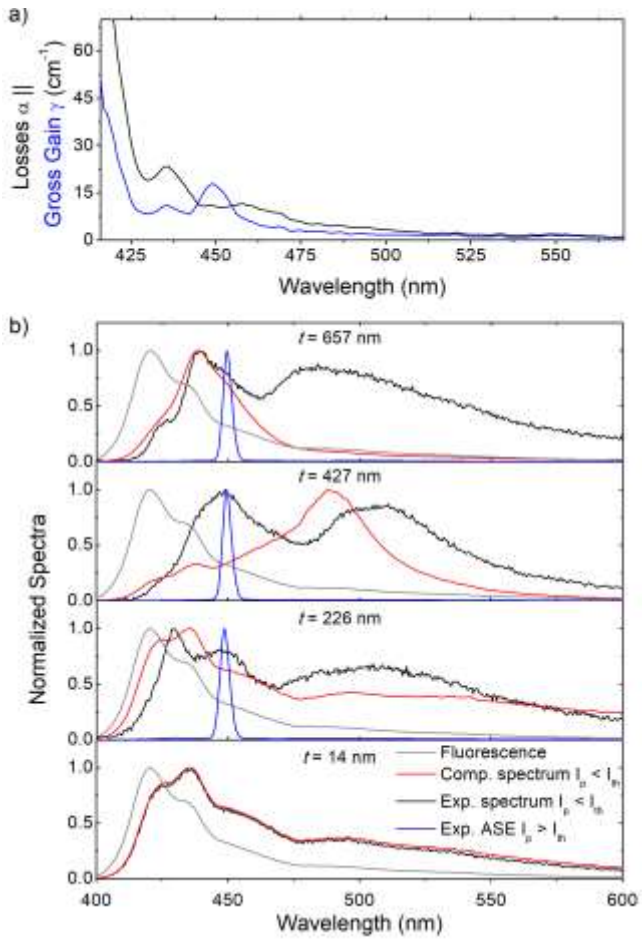

Figure 4: a) Losses coefficient and gross gain spectra for a film with thickness ~230 nm (sample S5). b) Experimental (black lines) and computed (red lines) spectra well-below threshold for PFO films of varying thicknesses *t*. The fluorescence spectrum (gray lines) and the ASE spectra above threshold (blue lines) have been included for comparison purposes. The sample with thickness t = 14 nm did not show ASE. The spectra in b) have been normalized by its maximum value.

Based on an improved version of the leaky-mode formalism described in ref. [35], we calculated the edge-emitted ASE spectra (well-below threshold) that should be detected from PFO films displaying, exclusively, leaky-modes (see Appendix B). It is obvious that their presence significantly changes the spectral shape of the edge-emitted light (Fig. 4b and S3). In the thinnest films (t <50 nm), the optical path between two consecutive reflections at the film/air and film/substrate interfaces is much smaller than the wavelength of the propagating field. Hence, the phase difference between the multiple beams tends to zero and will be almost the same for all wavelengths. This means that all of them will experience a similar level of constructive/destructive interference, and thus there will be a weak spectral modulation (Fig. 4b). As the waveguide thickness increases, the optical path inside

the film lengthens, giving place to larger differences in the phase changes gained by each wavelength. In this case, each of them will experience a different level of constructive/destructive interference and, thus, the edge-emitted spectra will display a strong spectral modulation (Fig. 4b). These changes are qualitatively consistent with what it is observed experimentally. Needless to say, the similitude is far from perfect, and this is ascribed to several factors. Firstly, the optical, structural, absorptive, and dispersive properties of the films, as well as the detection configuration that we have assumed are, probably, not exactly those of the measured films. Then, the light might not be emitted equally into the TE and TM modes (i.e., there might be emission anisotropy). And finally, we have assumed that there is only leaky-mode emission, but these PFO films sustain as well wave-guided modes [25], which modify the edge-emitted light in a different way. Experimentally both were detected, and there is no way to know how much each of them contributes to the total emission.

Another evidence for the presence of leaky-modes can be found in the position of the ASE emission band well-above threshold (Fig. 4b and S3). Attending to the sole presence of waveguided modes, the ASE peak should redshift steadily and monotonically while increasing the film thickness due to mode-confinement effects [3,31]. While the ASE peak wavelengths for our PFO samples show an increasing tendency with the thickness, they do it neither steadily nor monotonically (Fig. S4). These peak wavelength deviations from the expected trend could arise due to the presence of transmission resonances owed to leaky-modes.

All in all, the main conclusion that can be drawn from the previous analysis is that the anomalous resonance-like spectral features in both the losses and gross gain spectra (Fig. 4a) are completely normal and can be associated to the presence of leaky-modes.

3.3 Multiple species effects

There are occasions in which more than one emissive species are involved in the excitation/emission process. Namely, energy transfer pairs [36, 37, 38], coexistence of monomeric and aggregated forms (in the ground or the excited states) [27, 39, 40], or different crystalline phases

[41]. In these cases, each species has its own effective population inversion Δn that, presumably, depends on the pump intensity in a more complex manner than the one described by eq. (1b), overall if the species interact between each other. Since the VPI method formulation assumes a single type of emitter [23], it should not perform too well in samples with multiple species. To check its performance, we have analysed two different cases in which there are two emissive/absorptive species: One case corresponding to an energy transfer process between two types of molecules, and one case where the monomeric and aggregated forms of the same molecule coexist.

3.3.1 Förster Resonance Energy Transfer (FRET)

To check the performance of the VPI method on a sample displaying FRET, we chose a PMMA waveguide doped with Perylene Orange (PO) and Perylene Red (PR) [26]. In this sample, the energy transfer from PO to PR was not complete, and there was a non-negligible contribution of PO to the fluorescence emission. The complete fitting results and parameters of this sample can be found in the "Graphical Report" that has been appended to the Supplementary Material.

The shape of the fitted spectra is the one expected for this system (Fig. 5a). In particular, the losses spectrum displays a clearly defined band centred at 575 nm, which is coincidental with the absorption peak of PR [26]. As we move towards higher energies, the losses spectrum is mainly dominated by the PO absorption band tail. Nevertheless, even though the ASE spectra of this sample are very well behaved (see Graphical Report), the value and, overall, the uncertainty of the losses coefficient at the ASE peak (~ 620 nm) are much higher than expected (33 ± 8 cm^{-1}). This is the first evidence that suggests that the VPI method is not performing well. Another evidence is found in that the fitted ASE intensity at the peak wavelength is not very accurate (Fig. 5b), showing overestimations of more than a 20 % in the region where there is a change in slope (see relative error in Fig. 5b). In addition, the computed ASE threshold (dashed vertical line in Fig. 5b) is much lower than the one originally reported (58 vs. 115 kW cm^{-2}). Yet another evidence is that the fit suggests that at the lowest pump intensities there is a considerable level of amplification (gross gain $\gamma\Delta n \leq 10$ cm^{-1}), even when the FWHM shows no collapse at all (Fig. 5c). This is analogous to what happened

with the sample COPV6 8 wt % (Fig. 1c), but in this case there is not an imbalance between ASE spectra below and above threshold.

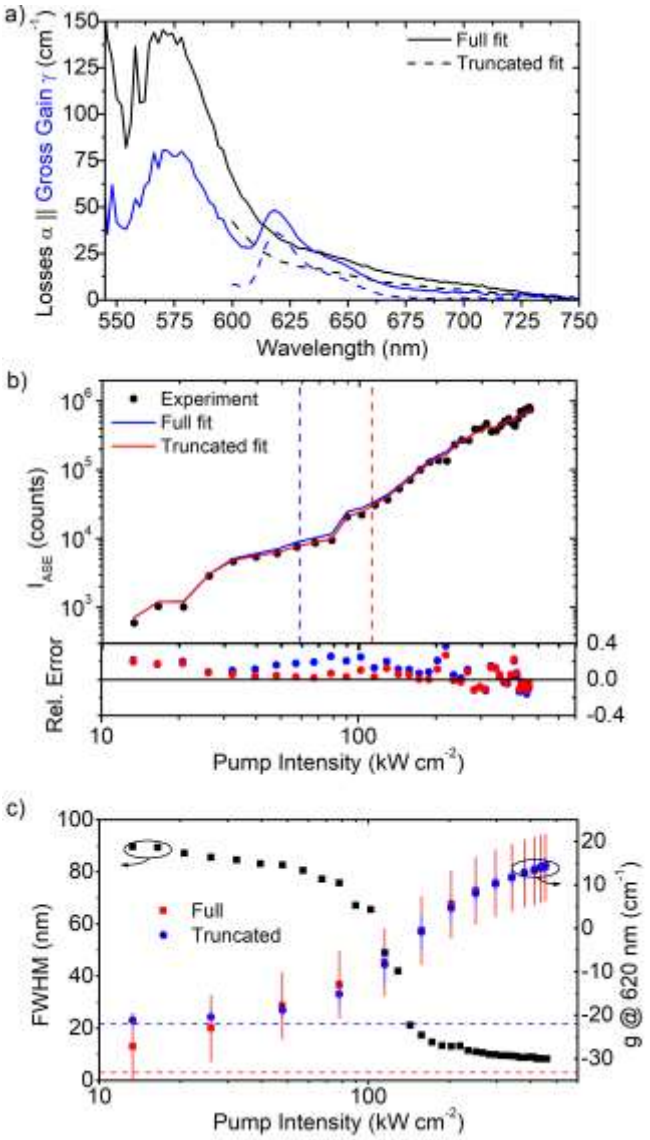

Figure 5: a) Losses coefficient and gross gain spectra for a PMMA film doped with a mixture PO/PR. b) Experimental (dots) and fitted (solid lines) ASE intensities and the corresponding relative error. The vertical dashed lines mark the computed ASE threshold position. c) FWHM (left) and fitted net optical gain *g* (right) as a function of pump intensity. The dashed horizontal lines represent $g = -\alpha$.

Does it mean that the VPI method can never be applied to analyse samples with active species undergoing energy transfer? Not exactly. The VPI method could be used if the effect of the donor over the fit is almost negligible. This may happen in two cases: when the FRET efficiency is

sufficiently high as to make the donor fluorescence to vanish, or truncating the fit to the spectral region where the gain of the donor is nullified, this is, to the emission window of the acceptor. We can exemplify the latter approach by repeating the fit for wavelengths above 600 nm, where the PO optical gain is low (Fig. 2 and Fig. 5a). As can be appreciated in Figs 5a and b, the fit is much better. The spectral shape for the losses and gross gain is very similar to the previous one, but the value and uncertainty of the losses coefficient at the ASE peak (~ 620 nm) are more consistent with what could be expected for this kind of samples (22 ± 2 cm^{-1}). The relative errors for the fitted ASE peak intensity are smaller (~5%) and the computed threshold is closer to the one originally reported (112 vs. 115 kW cm^{-2}). Finally, the g vs. I_p curve (Fig. 5c) does not show evidences anymore of strong amplification at the lowest pump intensities. In any case, it is not very recommended to follow this approach, as the function Δn (eq. 1b) might not be capturing the correct dependency.

3.3.2 Coexistence of monomers and aggregates in the excited-state

At the high dye concentrations used in dye-doped polymer waveguides, it is highly probable that the molecules come close enough as to form dimers or higher order aggregates. These aggregates are usually formed in the ground state, but they may be as well formed in the excited state, giving place to the so-called excimers or superexciplexes [27, 39]. Such is the case of some rosamines, a family of xanthene dyes that may display bichromatic emission, one high energy band corresponding to the monomeric form, and a lower energetic band that can be ascribed to the excimeric form [27]. To test the performance of the VPI method against materials with two emitting species, we analysed a pHEMA waveguide doped with rosamine at a concentration of 50 mM (compound **4** in original paper [27]). The complete fitting results and parameters of this sample can be found in the "Graphical Report" that has been appended to the Supplementary Material.

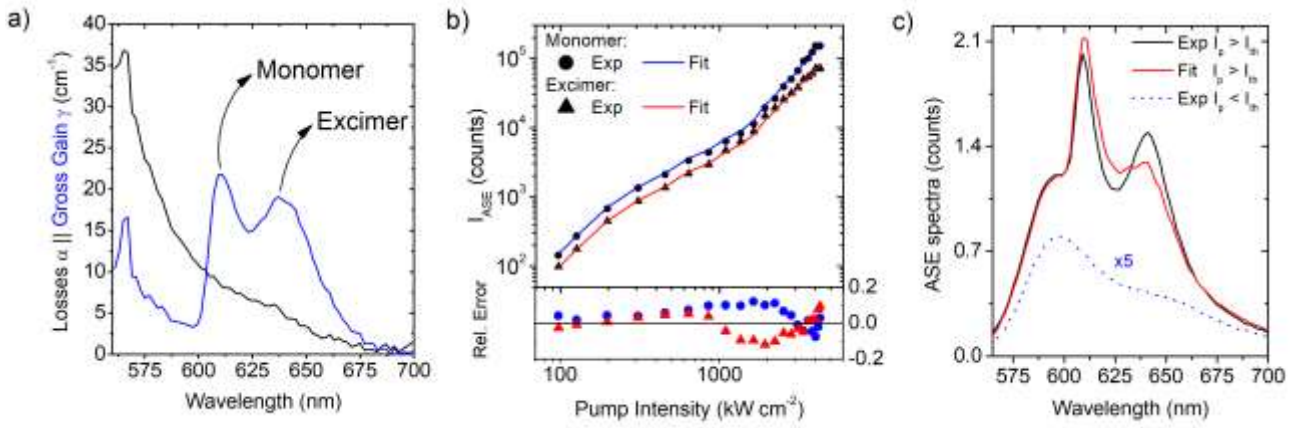

Figure 6: a) Losses coefficient and gross gain spectra for a pHEMA film doped with a rosamine. b) Experimental (dots) and fitted (solid lines) ASE intensities at the peak wavelength and the corresponding relative error. c) Experimental and fitted ASE spectra at a pump intensity I_p above threshold I_{th} (1.9 MW cm^{-2}). The ASE spectrum well-below threshold I_{th} (blue dotted line) has been included for comparison purposes.

The losses coefficient spectrum shows the exponential decay dependency with the wavelength that we are already familiar with (Fig. 6a). Unlike the sample with the PO/PR mixture, the value and uncertainty of the losses coefficient at the peak wavelength are not too high (8.1 ± 0.4 cm^{-1}). The gross gain spectrum shows two overlapping bands centred at 611 nm and 639 nm corresponding, respectively, to the monomers and the excimers. On first consideration, one may assume that the fit is not bad, as the errors associated to the fitting parameters are relatively low (see Graphical Report at SI). Nevertheless, the discrepancies arise when comparing the experimental and fitted ASE intensities at the monomer and excimer wavelengths (Fig. 6b). At low pump intensities the relative errors are small, but when the pump intensity approaches the threshold region the fit departs from the experimental values, overestimating the values of the monomer and underestimating the values of the excimer (in both cases by up to a 10%). The differences between the experiment and the fit are much better appreciated in the spectra for which both ASE bands are already well-defined (Fig. 6c). This plot suggests that the fit is not performing appropriately. Interestingly, the deviations of the fit with respect to the experimental values at both wavelengths follow a specular trend (Fig. 6b). That is, the fit overestimates the monomer intensities by approximately the same amount as it underestimates the

excimer ones (or the other way around). This is to be expected, though. As it was explained before, each emitting species would have its own properties (Ω, η, Δn, γ, and α in our context). Given that the VPI method assumes the existence of a single species, what it does is to find the average, over the two species, for those parameters. Accordingly, the fitted parameters (and thus the intensity) would be as far from the actual monomer parameters as they are from the excimer ones. Hence, the fitted parameters are not reliable either for the monomers or the excimers. Unfortunately, in this case we cannot resort to truncating the fit to the emission window of each species, as they are highly overlapped.

3.4 Excited State Absorption effects

The optical gross gain coefficient $\gamma(\lambda)$ retrieved from the VPI method (eq. (3)) explicitly accounts for the excited state absorption (ESA). Unfortunately, the nature of the method hinders the possibility of obtaining the precise shape and magnitude of the ESA spectrum. Nevertheless, we could infer its presence by looking for spectral distortions in $\gamma(\lambda)$ with respect to the sum of the ground state absorption spectrum and the stimulated emission spectrum, as the former should resemble the latter in the absence of ESA (cf. eq. (3)). To check the capability of the VPI method to extract information on the ESA, we have analysed a set of ASE spectra obtained from *anti*-$B_{18}H_{22}$ (see Methods), an inorganic cluster which, being the first boron hydride (or borane) displaying laser emission [28], suffers a strong ESA at the emission window that severely degrades its laser performance [42]. The complete fitting results and parameters of this sample can be found in the "Graphical Report" that has been appended to the Supplementary Material.

Although the gross gain can be negative whenever $\alpha_{ESA}(\lambda) > \alpha_{ST}(\lambda) + \alpha_{GSA}(\lambda)$ (cf. eq. (3)), it is usually assumed to be positive. In fact, the GUI *AgL* forces this condition by default ($\gamma(\lambda) \geq 0, \forall\lambda$). As is reported in the documentation, this assumption is reasonable for most cases, usually works fine and it is recommended to leave it like that. Otherwise, it can give spurious results. But if the fit renders several zero values for $\gamma(\lambda)$ or if there is a previous knowledge or suspicion that indicates that

$\gamma(\lambda)$ can be negative for some λ values, this constraint can be removed. This is in fact what we have done to analyse the ASE spectra obtained from *anti*-$B_{18}H_{22}$ solutions.

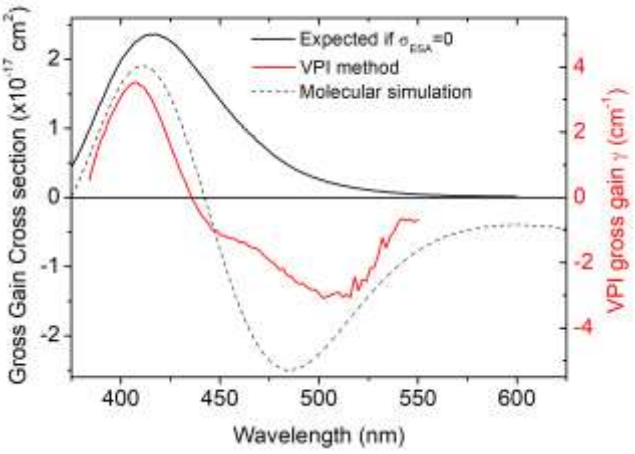

Figure 7: Experimental stimulated emission cross section σ_{ST} (black solid line), gross gain $\gamma(\lambda)$ obtained from the VPI method (red solid line), and gross gain cross section calculated by means of molecular simulations [42] (black dashed line).

The solutions of *anti*-$B_{18}H_{22}$ display a very large Stokes shift [43] and, thus, in the absence of ESA, the gross gain spectrum should resemble the stimulated emission cross section spectrum (Figure 7). In contrast, the gross gain spectrum obtained with the VPI method shows a strikingly different spectral shape. Not only the fitted gross gain shows a blue-shifted narrower amplification band, but it displays negative values in a wide spectral range. These evidences point out to the presence of a strong ESA resonant band whose magnitude is larger than the stimulated emission one at those wavelengths. The gross gain spectrum predicted by quantum chemistry computations [42] nicely matches the one obtained with the VPI method (Figure 7), providing strong evidences that the spectral distortions are due to ESA and not due to numerical or experimental artefacts.

Conclusions

The main goal of this manuscript was to show that the VPI method is a powerful and reliable tool that not only provides estimations for the losses and optical gains, but that opens the door to obtaining a huge amount of information about the physics involved in the excitation of ASE in active

waveguides and solutions as well as insights into the active media photophysics. And this goal has been largely fulfilled.

We have shown that using the VPI method and the GUI *AgL* to assess the ASE properties as a function of the active material concentration not only helps finding the optimal ASE operation conditions, but enables to determine, among other things, whether the losses at the ASE peak wavelength are dominated by modal/scattering effects or by ground state absorption. But the most fundamental teaching from this section is that to perform a good fit with the GUI *AgL* and thus be able to carry out comparative studies that are reliable and quantitative, it is essential to acquire a good number of ASE spectra in a wide range of pump values. Ideally, the ASE experiment should include evenly distributed spectra well-below threshold (negligible FWHM collapse), in the threshold region (steep change in FWHM), and well-above threshold (saturation in FWHM collapse).

We have shown that, contrary to what it is usually believed, the ASE threshold does not always correlate with the optical gain. For example, by modifying the active film thickness, one can modulate the ASE threshold by orders of magnitude while leaving the optical gain almost unchanged. Another key aspect is that the VPI method helps detecting the presence of leaky-modes through a quick inspection of the fitted spectra. Thus, the presence of resonance-like spectral features in both the losses and gross gain spectra could be indicative of this waveguiding effect (effects due to a lack of spectra well-below threshold should be ruled out first). Remarkably, the presence of leaky-mode resonances does not impose any restriction to the use of the VPI method and the GUI *AgL*, as they are accounted for implicitly (cf. eqs. (2) and (3)).

Since the VPI method formulation assumes a single type of emitter, it does not perform well in samples with multiple species (energy transfer, aggregates, …). For the energy transfer case, though, the VPI method could be used in two limiting cases for which the donor effect is negligible: when the transfer efficiency approaches unity or truncating the fit to the emission window of the acceptor (provided there is not much overlap). This last approach should be followed with care and its results should not be trusted blindly.

Finally, the inspection of the shape of the gross gain spectrum allows retrieving information about the excited state absorption without the need to resort to more costly pump/probe techniques. This particular result highlights the potential of the VPI method.

All the results presented in this manuscript highlight that the VPI method is a powerful and reliable tool that helps in comprehensibly characterizing the laser gain properties of waveguides and solutions.

Acknowledgments

The researchers from the University of Alicante and LC acknowledge financial support from the Spanish Ministerio de Economía y Competitividad (MINECO) and the European FEDER funds through Grant numbers MAT2015-66586-R and MAT2017-83856-C3-1, respectively.

Appendix A: Dependency of losses on the active medium concentration C

In order to understand the effects of the active medium concentration on the waveguide losses it is important to evidence that $\alpha_{GSA}(\lambda)$ is not the only parameter of the losses coefficient in eq. (2) affected by *C*. In particular, the confinement function $\Gamma(\lambda)$ not only accounts for all waveguiding effects, but it also reflects how well the pump density across the film spatially overlaps with the mode profile. Hence, $\Gamma(\lambda)$ depends on *C* through the variation of the pump density across the film. Nevertheless, we must stress that this effect will be less noticeable in dye-doped polymer films (where the concentration is usually low to avoid aggregation) than in neat or slightly diluted organic semiconductor thin films (where the pump absorption is usually stronger). That said, this effect can be accounted for by means of the pump to mode overlap (PMO) factor Γ_{PMO}, which is defined as [25, 44]:

$$\Gamma_{PMO} = \frac{\int_0^t e^{-\alpha_{GSA}(\lambda_p)z}|E(z,\lambda_{ASE})|^2 dz}{\int_{-\infty}^{\infty}|E(z,\lambda_{ASE})|^2 dz} \quad \text{(A1)}$$

In eq. (A1), *z* is the coordinate across the film, $E(z,\lambda_{ASE})$ is the electric field distribution of the propagating mode, and *t* is the film thickness. Note that α_{GSA} is evaluated at the pump wavelength

(λ_p), and $E(z,\lambda_{ASE})$ at the ASE propagating wavelength. With $\alpha_{GSA}(\lambda_p)$ and $E(z, \lambda_{ASE})$ known, eq. (A1) can be used to compute $\Gamma_{PMO}(C)$, *i.e*, the dependency of the pump to mode overlap on the active medium concentration. Finally, it is easy to see that the losses coefficient $\alpha(\lambda)$ depends on C as:

$$\alpha(\lambda_{ASE}, C) = (\alpha_{SC}(\lambda_{ASE}) + \nu \cdot C) \cdot \Gamma_{PMO}(C) \quad \text{(A2)}$$

where ν is a proportionality factor (cf. eq. (2)). If C is expressed in units of M (molar concentration), then ν equals ε·ln(10), with ε the molar extinction coefficient.

Given that $\Gamma_{PMO}(C)$ decays (almost to perfection) exponentially with the concentration, the non-linearity of eq. (A2) can be empirically approximated by the following expression:

$$\alpha(\lambda_{ASE}, C) = (\alpha_0 + \alpha_1 C)e^{-C/C_0} \quad \text{(A3)}$$

Where α_0 and α_1 are positive parameters and C_0 is an exponent that determines how much the losses deviates from the expected linear increase with C. The parameters in eq. (A3) will depend on the combination of gain material and waveguide structure. For instance, in the samples based on COPV6, the theoretically predicted value of C_0 amounts to ~50 wt % (for C_{COPV6} expressed in wt %). To obtain this estimation, the $\alpha_{GSA}(\lambda_p)$ values at each concentration were obtained directly from ref. [24], and the waveguide mode profiles $E(z, \lambda_{ASE}$ = 580 nm) were computed with an online mode solver for slab waveguides [45] (assuming a 600 nm thick polystyrene thin film (n_f=1.6) deposited on top of a quartz substrate (n_s=1.45) [24]). These parameters were used to compute, as a function of the concentration, the pump to mode overlaps (eq. A1) and the theoretically predicted losses (eq. A2). C_0 was retrieved from the fit of eq. (A3) to the latter values.

Appendix B. Leaky-mode analysis

The presence and effects of leaky-modes (LM) in the PFO thin films of different thicknesses has been investigated using an improved version of the formalism described in ref. [35]. Firstly, we determined that the leaky-mode contribution ($\Gamma_{LM}(\lambda)$) to the mode confinement function assumed in the VPI method ($\Gamma(\lambda)$ in eqs. 2 and 3), is the reciprocal of the in-substrate transmission [35]. Concerning the improvements, we observed that the previous leaky-mode analysis assumes that the

film is transparent, an approximation that does not hold true for the PFO films. The presence of absorption modifies the total phase change upon one reflection at both the film/air and film/substrate interfaces. This extra phase change can be accounted for with $i\alpha_{GSA}(\lambda)L_{path}$, where $\alpha_{GSA}(\lambda)$ is the ground state absorption coefficient and L_{path} is the distance travelled after two reflections. Moreover, in order to reproduce the experimental conditions under which the PFO ASE spectra were collected, the following factors were taken into account to calculate $\Gamma_{LM}(\lambda)$: a) PFO is anisotropic both in refractive index and absorption [46]; b) a lens was used to collect the edge-emitted light and thus one must integrate over several transmission angles (±5º around the waveguide plane); and c) the light was emitted without a distinct polarization, and thus 50% went to the TE-mode and 50% to the TM-mode. Finally, the edge-emitted ASE spectra well-below threshold can be simulated using the expression:

$$I_{ASE}(L, I_p \to 0, \lambda) \propto \frac{F(\lambda)}{\Gamma_{LM}(\lambda)\alpha_{GSA}(\lambda)}\left(1 - e^{-\Gamma_{LM}(\lambda)\alpha_{GSA}(\lambda)L}\right) \quad \text{(B1)}$$

where $\alpha_{GSA}(\lambda)$ is the ground state absorption coefficient and $\Gamma_{LM}(\lambda)$ is the calculated leaky-mode confinement function. Eq. (B1) is the expression to estimate the losses coefficient in the VPI method [23] but with the total losses $\alpha(\lambda)$ substituted by $\Gamma_{LM}(\lambda)\alpha_{GSA}(\lambda)$. This substitution entails assuming that there are only absorptive losses (cf. eq. (3)) and that there are no other waveguiding effects apart from leaky-modes.

Appendix C. Supplementary Material

It contains supplementary figures for section 3.2 and all the "Graphical Reports" with the complete fitting results and parameters for the samples analysed in this manuscript.

References

[1] C. Grivas, M. Pollnau, Organic solid-state integrated amplifiers and lasers, Laser Photonics Rev. 6 (2012) 419-462

[2] A.J.C. Kuehne, M.C. Gather, Organic Lasers: Recent Developments on Materials, Device Geometries, and Fabrication Techniques, Chem. Rev. 116 (2016) 12823-12864

[3] M. Anni, S. Lattante (Eds.), Organic Lasers: Fundamentals, Developments, and Applications, Pan Stanford Publishing, Singapore, 2018

[4] A.S. D. Sandanayaka, T. Matsushima, F. Bencheikh, S. Terakawa, W. J. Potscavage Jr., C. Qin, T. Fujihara, K. Goushi, J.-C. Ribierre, C. Adachi, Indication of current-injection lasing from an organic semiconductor, Appl. Phys. Express 12 (2019) 061010

[5] T. Kanagasekaran, H. Shimotani, K. Kasai, S. Onuki, R. D. Kavthe, R. Kumashiro, N. Hiroshiba, T. Jin, N. Asao, K. Tanigaki, Towards electrically driven organic semiconductor laser with field-effective transistor structure, 2019, arXiv: 1903.08869v2 [physics.optics]

[6] C. Dang, J. Lee, C. Breen, J. S. Steckel, S. Coe-Sullivan, A. Nurmikko, Red, green and blue lasing enabled by single-exciton gain in colloidal quantum dot films, Nat. Nanotechnol. 7 (2012) 335-339

[7] Y. Ye, Z. Jing Wong, X. Lu, X. Ni, H. Zhu, X. Chen, Y. Wang, X. Zhang, Monolayer excitonic laser, Nature Photon. 9 (2015) 733-737

[8] C. Grivas, Optically pumped planar waveguide lasers: Part II: Gain media, laser systems, and applications, Prog. Quantum Electron. 45-46 (2016) 3-160

[9] P. Geiregat, A. Houtepen, L. Sagar, I. Infante, F. Zapata, V. Grigel, G. Allen, C. Delerue, D. Van Thourhout, Z. Hens, Continuous-wave infrared optical gain and amplified spontaneous emission at ultralow threshold by colloidal HgTe quantum dots, Nat. Mater. 17 (2018) 35-42

[10] M M. Stylianakis, T. Maksudov, A. Panagiotopoulos, G. Kakavelakis, K. Petridis, Inorganic and Hybrid Perovskite Based Laser Devices: A Review, Materials 12 (2019) 859

[11] V. Bonal, R. Muñoz-Mármol, F. Gordillo Gámez, M. Morales-Vidal, J. M. Villalvilla, P. G. Boj, J. A. Quintana, Y. Gu, J. Wu, J. Casado, M. A. Díaz-García, Solution-processed nanographene distributed feedback lasers, Nat. Commun. 10 (2019) 3327

[12] E. R. Martins, Y. Wang, A. L. Kanibolotsky, P. J. Skabara, G. A. Turnbull, I. D. W. Samuel, Low- Threshold Nanoimprinted Lasers Using Substructured Gratings for Control of Distributed Feedback, Adv. Opt. Mater. 1 (2013) 563-566

[13] J. A. Quintana, J. M. Villalvilla, M. Morales-Vidal, P. G. Boj, X. Zhu, N. Ruangsupapichat, H. Tsuji, E. Nakamura, M. A. Díaz-García, An Efficient and Color-Tunable Solution-Processed Organic Thin-Film Laser with a Polymeric Top-Layer Resonator, Adv. Optical Mater. 5 (2017) 1700238

[14] A. S. D. Sandanayaka, T. Matsushima, F. Bencheikh, K. Yoshida,M. Inoue, T. Fujihara, K. Goushi, J.-C. Ribierre, C. Adachi, Toward continuous-wave operation of organic semiconductor lasers, Science Advances 3 (2017) e1602570

[15] N. Tsutsumi, K. Kaida, K. Kinashi, W. Sakai, High-Performance All-Organic DFB and DBR Waveguide Laser with Various Grating Height Fabricated by a Two-Photon Absorption DLW Method, Sci. Rep. 9 (2019) 10582

[16] V. Bonal, J. A. Quintana, J. M. Villalvilla, P. G. Boj, M. A. Díaz-García, Controlling the emission properties of solution-processed organic distributed feedback lasers through resonator design, Sci. Rep. 9 (2019) 11159

[17] Q. Zhang, Q. Wei, X. Guo, G. Hai, H. Sun, J. Li, R. Xia, Y. Qian, S. Casado, J.R. Castro-Smirnov, J. Cabanillas-Gonzalez, Concurrent Optical Gain Optimization and Electrical Tuning in Novel Oligomer: Polymer Blends with Yellow-Green Laser Emission, Advanced Science, 6 (2019) 1801455

[18] F. Vogelbacher, M. Sagmeister, J. Kraft, X. Zhou, J. Huang, M. Li, K.J. Jiang, Y. Song, K. Unterrainer, R. Hainberger, Slot-Waveguide Silicon Nitride Organic Hybrid Distributed Feedback Laser, Sci. Rep. 9 (2019) 18438

[19] S. Ma, M. Wei, S. K. Rajendran, M. Karl, B. Xu, M. C. Gather, W. Tian, G. A. Turnbull, I. D. W. Samuel, Pick and Place Distributed Feedback Lasers Using Organic Single Crystals, Adv. Opt. Mater. 8 (2020)1901785

[20] K.L. Shaklee, R.F. Leheny, Direct determination of optical gain in semiconductor crystals, Appl. Phys. Lett. 18 (1971) 475-477

[21] L. Cerdán, A. Costela, I. García-Moreno, On the characteristic lengths in the variable stripe length method for optical gain measurements, J. Opt. Soc. Am. B 27 (2010) 1874-1877

[22] L. Cerdán, Variable Stripe Length method: influence of stripe length choice on measured optical gain Opt. Lett. 42 (2017) 5258-5261

[23] L. Cerdán, Simultaneous retrieval of optical gains, losses, and threshold in active Waveguides, Opt. Laser Technol. 121 (2020) 105814

[24] M. Morales-Vidal, P. G. Boj, J. M. Villalvilla, J. A. Quintana, Q. Yan, N.-T. Lin, X. Zhu, N. Ruangsupapichat, J. Casado, H. Tsuji, E. Nakamura, M. A. Díaz-García, Carbon-bridged oligo(p-phenylenevinylene)s for photostable and broadly tunable, solution-processable thin film organic lasers, Nat. Commun. 6 (2015) 8458

[25] M. Anni, A. Perulli, G. Monti, Thickness dependence of the amplified spontaneous emission threshold and operational stability in poly(9,9-dioctylfluorene) active waveguides, J. Appl. Phys. 111 (2012) 093109

[26] L. Cerdán, A. Costela, G. Durán-Sampedro, I. García-Moreno, M. Calle, M. Juan-y-Seva, J. de Abajo, G. A. Turnbull, New perylene-doped polymeric thin films for efficient and long-lasting lasers, J. Mater. Chem. 22 (2012) 8938

[27] L. Cerdán, V. Martínez-Martínez, I. García-Moreno, A. Costela, M.E. Pérez-Ojeda, I. López Arbeloa, L. Wu, K. Burgess, Naturally Assembled Excimers in Xanthenes as Singular and Highly Efficient Laser Dyes in Liquid and Solid Media, Adv. Opt. Mater 1 (2013) 984-990

[28] L. Cerdán, J. Braborec, I. García-Moreno, A. Costela, M. G. S. Londesborough, A borane laser, Nat. Commun. 6 (2015) 5958

[29] K. Kazlauskas, G. Kreiza, E. Radiunas, P. Adomenas, O. Adomeniene, K. Karpavicius, J. Bucevicius, V. Jankauskas, S. Jursenas, Concentration effects on spontaneous and amplified emission in benzo[c]fluorenes, Phys. Chem. Chem. Phys. 17 (2015) 12935

[30] F. Vogelbacher, X. Zhou, J. Huang, M. Li, K.-J. Jiang, Y. Song, K. Unterrainer, R. Hainberger, Material gain concentration quenching in organic dye-doped polymer thin films, Opt. Mater. Exp. 9 (2019) 1208-1222

[31] E. M. Calzado, M. G. Ramírez, P. G. Boj, M. A. Díaz García, Thickness dependence of amplified spontaneous emission in low-absorbing organic waveguides, Appl. Opt. 51 (2012) 3287-3293

[32] E. M. Calzado, J. M. Villavilla, P. G. Boj, J. A. Quintana, V. Navarro-Fuster, A. Retolaza, S. Merino, M. A. Díaz García, Influence of the excitation area on the thresholds of organic second-order distributed feedback lasers, Appl. Phys. Lett. 101 (2012) 223303

[33] R. Xia, G. Heliotis, Y. Hou, D. D. C. Bradley, Fluorene-based conjugated polymer optical gain media, Org. Electron. 4 (2003) 165-177

[34] T. Kawase, D. J. Pinner, R. H. Friend, T. Shimoda, Grazing emitted light from films of derivative polymer of polyfluorene, Synth. Met. 111-112 (2000) 583-586

[35] A. Penzkofer, W. Holzer, H. Tillmann, H.-H. Hörhold, Leaky-mode emission of luminescent thin films on transparent substrates, Opt. Commun. 229 (2004) 279-290

[36] L. Cerdán, A. Costela, I. García-Moreno, Waveguided random lasing in red-emitting-dye-doped organic–inorganic hybrid polymer thin films, Org. Electron. 13 (2012) 1463-1469

[37] M. Umair Hassan, Y.- C. Liu, H. Butt, K. ul Hasan, J.- F. Chang, A. A. Olawoyn, R. H. Friend, Low thresholds for a nonconventional polymer blend—Amplified spontaneous emission and lasing in $F8_{1-x}$:SY_x system, J. Poly. Sci. Part B. Polym. Phys. 54 (2016) 15-21

[38] Q. Zhang, Q., J. Liu, Q. Wei, X. Guo, Y. Xu, R. Xia, L. Xie, Y. Qian, C. Sun, L. Lüer, J. Cabanillas-Gonzalez, D.D.C. Bradley, W. Huang, Host Exciton Confinement for Enhanced Förster-TransferBlend Gain Media Yielding Highly Efficient Yellow-Green Lasers, Adv. Funct. Mater. 28 (2018) 1705824

[39] V. Masilamani, A.S. Aldwayyan, Structural and solvent dependence of superexciplex, Spectrochim. Acta Part A 60 (2004) 2099

[40] L. Cerdán, A. Costela, G. Durán-Sampedro, I. García-Moreno, Random lasing from sulforhodamine dye-doped polymer films with high surface roughness, Appl. Phys. B 108 (2012) 839-850

[41] M. Anni, Dual band amplified spontaneous emission in the blue in Poly(9,9-dioctylfluorene) thin films with phase separated glassy and β-phases, Opt. Mater. 96 (2019) 109313

[42] L. Cerdán, A. Francés-Monerris, D. Roca-Sanjuan, J. Bould, J. Dolansky, M. Fuciman, M. G. S. Londesborough, Unveiling the role of upper excited electronic states in the photochemistry and laser performance of *anti*-$B_{18}H_{22}$, J. Mater. Chem. C 8 (2020), 12806-12818.

[43] M. G. S. Londesborough, D. Hnyk, J. Bould, L. Serrano-Andrés, V. Sauri, J. M. Oliva, P. Kubat, T. Polivka, K. Lang, Distinct Photophysics of the Isomers of $B_{18}H_{22}$ Explained, Inorg. Chem. 51 (2012) 1471-1479

[44] I. Gozhyk, M. Boudreau, H. Rabbani Haghighi, N. Djellali, S. Forget, S. Chenais, C. Ulysse, A. Brosseau, R. Pansu, J.-F. Audibert, S. Gauvin, J. Zyss, M. Lebental, Gain properties of dye-doped polymer thin films, Phys. Rev. B 92 (2015) 214202

[45] 1-D mode solver for dielectric multilayer slab waveguides; https://www.computational-photonics.eu/oms.html (Last accessed: October 2020)

[46] B. P. Lyons, A. P. Monkman, A comparison of the optical constants of aligned and unaligned thin polyfluorene films, J. Appl. Phys. 96 (2004) 4735